Hindawi
International Journal of Energy Research
Volume 2024, Article ID 6616423, 10 pages
https://doi.org/10.1155/2024/6616423

Research Article

Nucleation-Controlled Production of Sub-50 nm Carbon Nanotubes through Electrochemical Conversion of Carbon Dioxide in Carbonate Molten Salt

Min Woo Park and Chan Woo Lee

Department of Chemistry, Kookmin University, Seoul 02707, Republic of Korea

Correspondence should be addressed to Chan Woo Lee; cwlee1@kookmin.ac.kr

Received 7 November 2023; Revised 27 March 2024; Accepted 3 April 2024; Published 24 April 2024

Academic Editor: Adrian Loy Chun Minh

The increasing emission of carbon dioxide worldwide has emerged as a major global concern in the context of addressing climate change. Converting CO_2 to high-value carbon materials is a promising solution to capture emitted carbon for achieving carbon neutrality. Furthermore, such conversion can provide carbon nanomaterials for key industries, including the lithium battery and fuel cell industries. Here, it is shown that sub-50 nm tangled carbon nanotubes (CNTs) can be synthesized by adjusting the metaborate concentration and the current density through the electrochemical conversion of carbon dioxide in a molten carbonate salt. The metaborate ion concentration affects the product selectivity and carbon morphology, and the current density is strongly related to the particle size of *in situ* seed catalysts supplied by the dissolution of an Ni-Fe-Cr alloy anode. The optimized process conditions control the nucleation and growth of carbon *via* a tip-growth mechanism, thereby promoting the formation of sub-50 nm CNTs rather than bulky irregular carbon particles. The Raman and Brunauer–Emmett–Teller analyses showed that the properties of the prepared CNTs depended on the synthetic parameters. This study provides deep insights into the mechanism underlying carbon synthesis through the electrochemical reduction of a molten carbonate salt.

1. Introduction

The emission of carbon dioxide (CO_2) has steadily increased over the past few centuries, with CO_2 being unequivocally implicated as the primary driver of the worsening global climate change. There have been numerous discussions on technologies that involve the use of CO_2 to produce high-value chemicals. Among the technologies, molten salt-based CO_2 conversion technology is particularly promising [1, 2]. In molten salt electrolyte system, the molten salt exhibits significantly high electrical conductivity [3, 4]. Furthermore, molten salt electrolytes have high ability to absorb CO_2 molecules in the form of carbonate salts, which renders them well suited for handling CO_2 and facilitating its reaction. The products formed during molten salt electrolysis are carbon, carbon monoxide (CO), and oxygen (O_2); thus, molten salts are ecofriendly [5–9].

Molten salt-based CO_2 conversion can be used to convert CO_2 into valuable chemicals and substances, including CO, hollow carbon spheres, graphene, carbon nanofibers (CNFs), and carbon nanotubes (CNTs) [1, 10–14]. Among these substances, CNTs not only have substantial market value but also are widely used in various industries, for instance, in cement [15, 16], construction materials [15], batteries, capacitors, sensors [17], and textiles [15, 17]. Currently, the market share of CNTs is estimated at approximately $685.3 million, with CNT production facilities continuously expanding worldwide [18]. CNTs exhibit superior properties: low weight, high surface area, high electrical and thermal conductivities, and good mechanical properties. CNTs currently used in industrial sectors have an electrical resistance ranging from 5 to 50 $\mu\Omega$, a specific surface area ranging from 10 to 1000 $m^2 g^{-1}$, a diameter in the range of 2 to 100 nm, and G/D ratios ranging from 0.5 to 58.8. CNTs

used in lithium batteries are designed to have a small diameter (5 to 100 nm) and a large specific surface area below 400 $m^2 g^{-1}$ for better dispersion. If CNTs are to be employed as an active material in Li batteries, the lithium-ion intercalation capacity should be substantial, and the ion exchange rate should be high. CNTs possess a tubular structure that provides ample internal space for lithium-ion intercalation, and their external surface is electrochemically active, rendering them suitable for use as an active material in Li batteries. It is noteworthy that the diffusion of lithium ions plays a pivotal role in determining the performance of Li batteries, and as the length of CNTs decreases, ion diffusion becomes more facile, resulting in the enhanced capacity and performance of Li batteries. Furthermore, a reduction in the CNT diameter leads to higher performance in terms of the lithium-ion absorption energy [19–24].

It has been reported that the precise control of reaction conditions, such as the seed catalyst size, reaction time, electrolyte composition, electrode geometry, and electrode composition, in molten salt-based CO_2 conversion can facilitate the production of CNTs in various forms, such as multiwalled carbon nanotubes (MWCNTs), tangled CNTs, and CNT wool [15, 25–28]. To satisfy the requirements for certain applications of CNTs, researchers have devoted considerable effort to finely tune the properties of CNTs. CNTs with a diameter in the range from 500 to 22 nm can be prepared by controlling the size of the metal (or metal oxide) seed catalyst responsible for CNT nucleation and by changing the type of alkali metals in the electrolyte. Increasing the reaction time from 3 to 60 min also facilitates the growth of CNTs with a diameter between 13 and 22 nm [25]. It has also been reported that the morphology of synthesized carbon materials depends on the geometric structure (foil, foam, or wire) and metal composition (whether Ni, Fe, or Pt is present) of the electrodes [29, 30]. Additionally, the addition of oxide materials to the electrolyte has been shown to yield CNTs with high crystallinity at high current densities. In particular, borate can be introduced to increase the conductivity of CNTs [2, 13, 25, 26, 28, 29, 31–40].

In this paper, it is shown that sub-50 nm CNTs can be successfully prepared by controlling the current density and the electrolyte composition. Different concentrations of borate were added to the electrolyte to investigate the effect of borate concentration on the carbon morphology and the Faradaic efficiency (FE) for carbon production. Furthermore, the dimensions of CNTs (or CNFs) were found to strongly depend on the current density. Transmission electron microscopy (TEM) and scanning electron microscopy (SEM) analyses suggested that the seed catalysts, which were supplied *in situ* by an anodic reaction and deposited on the cathode side, acted as active sites for the nucleation and growth of CNTs. Controlling the synthesis conditions can help produce CNT materials with an average diameter of 26 nm, a specific surface area of 1136.9 $m^2 g^{-1}$, and a G/D ratio of 0.55. CNT materials with a small diameter and a high surface area are suitable for use in lithium battery application.

2. Experimental

2.1. Materials. Lithium carbonate (Li_2CO_3, 98.0%, Daejung), lithium chloride (LiCl, 98.0%, Daejung), and lithium metaborate ($LiBO_2$, 99.9%, Thermo Scientific) were used as electrolyte components. Sodium carbonate (Na_2CO_3, 99.0%, Daejung), potassium carbonate (K_2CO_3, 99.5%, Daejung), and silver sulfate (Ag_2SO_4, 99.5%, Daejung) were used as internal electrolyte components of a homemade reference electrode. A nickel sheet (0.2 mm thick) and Inconel 718 (0.3 mm thick) were used as the working electrode and counter electrode, respectively.

2.2. Electrochemical Measurements. All electrochemical measurements were conducted in an alumina crucible placed in a furnace. Pure CO_2 (50 mL/min) flow was maintained during the entire process. The Li_2CO_3-LiCl (68.8 : 31.2 mol%) electrolyte containing different concentrations of $LiBO_2$ was dried at 200°C under vacuum conditions before being heated. Lithium chloride was added to lower the temperature based on the phase diagram [41]. A Ni sheet cathode (contact area of 4.5 cm^2) was used as the working electrode, and an Inconel 718 anode (contact area of 9 cm^2) was the counter electrode. A homemade Ag/Ag_2SO_4 (0.1 mol/kg Ag_2SO_4) reference electrode filled with a Li-Na-K carbonate (43.5 : 31.5 : 25 mol%) internal electrolyte and sealed with a silver wire (1 mm in diameter) in a one closed-end alumina tube was used. Before the electrochemical measurements, the working electrodes were polished using sandpaper and were washed by ultrasonication in deionized water, acetone, and ethanol. Cyclic voltammetry (CV) and chronopotentiometry (CP) were performed using an electrochemical workstation (Ivium-n-Stat, Ivium Technologies B.V., Netherlands).

2.3. Product Purification. The raw products were collected from the working electrode after the cooling process, washed by ultrasonication in dilute hydrochloric acid to remove the hardened electrolyte and other impurities, and then filtered using a vacuum filter with 0.2 μm pore size filter paper. The products were then dried overnight at 60°C.

2.4. Characterization. Scanning electron microscope (SEM) images were recorded using a scanning electron microscope (JSM-7410F, JEOL Ltd., Japan) equipped with an energy dispersive X-ray spectrometer (EDS). Transmission electron microscope (TEM) images were obtained using a transmission electron microscope (JEM-2100F, JEOL Ltd., Japan) with an EDS. The Brunauer–Emmett–Teller (BET) analysis was conducted using an ASAP 2460 (Micromeritics, Korea) surface area and porosity analyzer. The Raman spectra of carbon under different conditions were acquired under laser excitation at 633 nm.

3. Results and Discussion

Figure 1(a) shows a schematic of chemical reactions that could have occurred (on the basis of previous reports) in the molten salt-based CO_2 electrolysis [6, 7, 39]. At the cathode, CO_3^{2-} contained in the Li_2CO_3-LiCl-$LiBO_2$ molten salt electrolyte (66.7 : 30.3 : 3.0 mol%) was electrochemically reduced to carbon (Eq. (1)). Carbonate reduction to CO also occurred as a major competing reaction (Eq. (2)). At the anode, the O^{2-} species in the electrolyte was oxidized, resulting in oxygen gas being produced (Eq. (3)). It has been

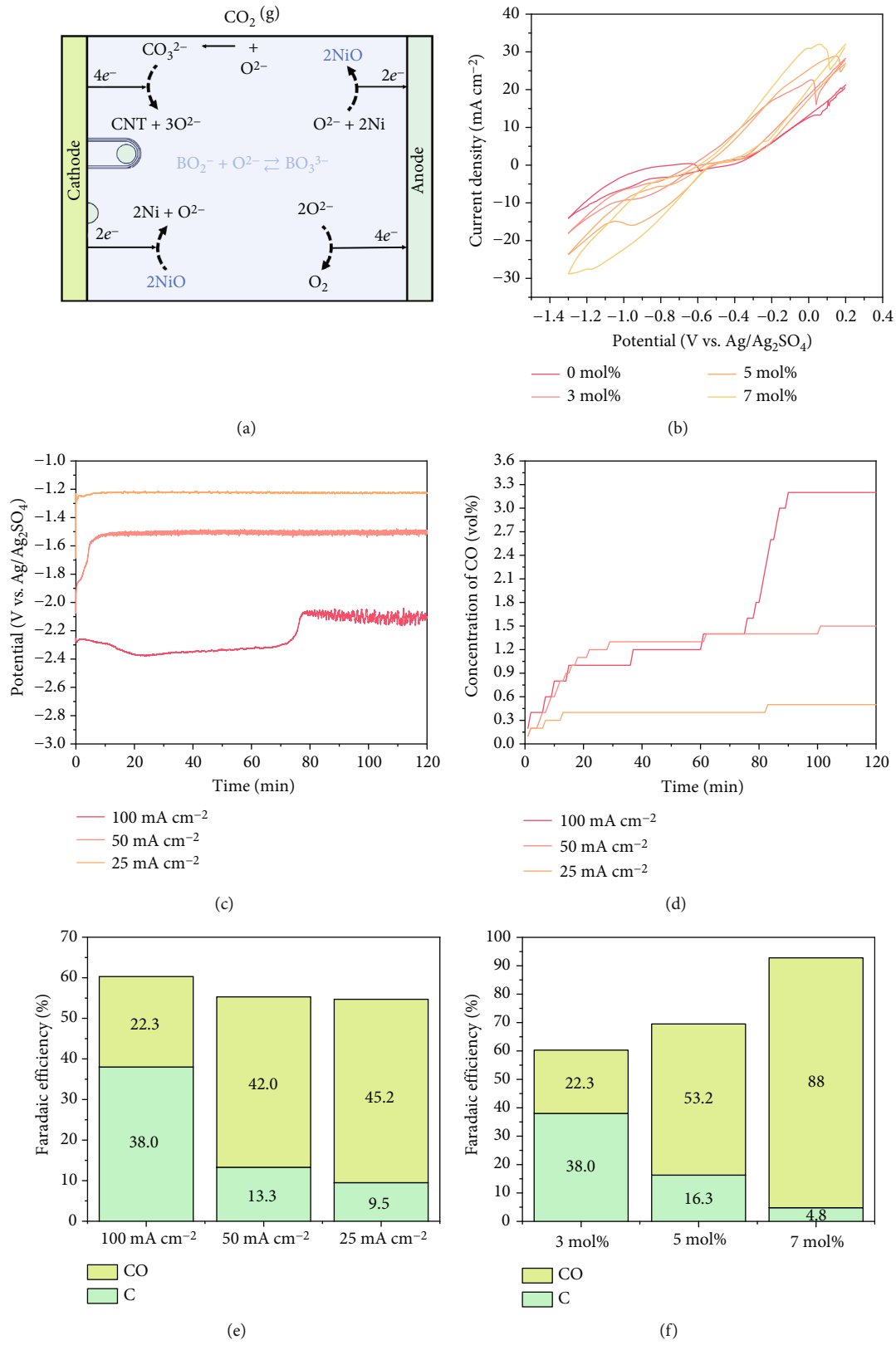

Figure 1: (a) Schematic of chemical reactions in the molten salt-based CO_2 electrolysis. (b) Cyclic voltammograms of the Ni working electrode measured for different borate concentrations at a scan rate of 10 mV s^{-1}. The (c) potential and (d) CO concentration monitored during 2 h of chronopotentiometry at current densities of 25, 50, and 100 mA cm^{-2} and a borate concentration of 3 mol%. (e) FEs for CO and carbon production at different current densities for a borate concentration of 3 mol%. (f) The effect of borate concentration on the FE at a current density of 25 mA cm^{-2}.

reported that anodic corrosion of metal electrodes occurs as shown in Eq. (4) [39]. The metal ions could have migrated toward the cathode and could have been deposited on it to form a metal seed catalyst at the cathode surface. The seed catalyst could have facilitated the nucleation and growth of carbon. When a borate additive (BO_2^-) was added to the molten salt electrolyte, BO_2^- would have played a pivotal role in controlling the concentration of O^{2-} ions owing to the existence of chemical equilibrium between BO_2^- and BO_3^{3-} as shown in Eq. (5) [6]. Furthermore, CO_2 molecules would have reacted with O^{2-} in the electrolyte to regenerate CO_3^{2-} (Eq. (6)).

$$\text{Cathode}: CO_3^{2-} + 4e^- \rightleftarrows C + 3O^{2-} \quad (1)$$

$$\text{Cathode}: CO_3^{2-} + 2e^- \rightleftarrows CO + 2O^{2-} \quad (2)$$

$$\text{Anode}: 2O^{2-} \rightleftarrows O_2 + 4e^- \quad (3)$$

$$\text{Anode}: Ni + O^{2-} \rightleftarrows NiO + 2e^- \quad (4)$$

$$\text{Electrolyte}: BO_2^- + O^{2-} \rightleftarrows BO_3^{3-} \quad (5)$$

$$\text{Electrolyte}: CO_2 + O^{2-} \rightleftarrows CO_3^{2-} \quad (6)$$

The electrochemical reactions involved in the molten salt-based CO_2 conversion were investigated by performing cyclic voltammetry analysis at a scan rate of 10 mV s^{-1} in the Li_2CO_3-LiCl-$LiBO_2$ molten salt electrolyte (66.7 : 30.3 : 3.0 mol%) under CO_2 flow of 50 mL min^{-1} at 750°C. The Ni foil and Inconel 718 (Ni-Fe-Cr alloy) electrodes were used as the working and counter electrodes, respectively. As shown in Figure 1(b), the cathodic current gradually increased from -0.5 to -1.3 V vs. Ag/Ag_2SO_4. This reduction reaction can be assigned to the reduction of CO_3^{2-} [6]. At high borate concentrations, a reduction peak at approximately -0.9 V vs. Ag/Ag_2SO_4 was prominent, and the peak has previously been reported to indicate borate-involved reduction of CO_3^{2-} [6]. It appears at a more positive potential compared with the CO_3^{2-} reduction peak.

In a reverse scan, without borate addition, anodic reaction started from -0.3 V vs. Ag/Ag_2SO_4 and subsequently increased at more positive potentials. The reaction involved is known to represent the oxidation of the deposited carbon and the Ni contained in the Inconel 718 anode [6, 39, 42]. However, in the presence of the borate additive, the oxidation reaction occurred at a shifted potential of -0.6 V vs. Ag/Ag_2SO_4. The current density values from -0.6 to -0.3 V vs. Ag/Ag_2SO_4 were quite similar, regardless of the borate concentration and the amount of charge accumulated during the cathodic cycling in the potential range from -0.6 to -1.3 V vs. Ag/Ag_2SO_4. It is likely that the potential shift originated from the anodic oxidation of Ni foil, as previously reported [39]. On the other hand, above -0.3 V vs. Ag/Ag_2SO_4, the oxidation current increased with the borate concentration, indicating that deposited carbon was oxidized above that potential. These results indicated that borate not only facilitated carbonate reduction but also enhanced metal oxidation in the molten salt-based electrochemical system.

Figure 1(c) shows a potential vs. time plot obtained during chronopotentiometry at current densities of 25, 50, and 100 mA cm^{-2} in the presence of 3 mol% borate. The potential became more negative as the current density increased, with higher overpotentials being required for carbonate reduction. On-line gas analysis was performed using a gas analyzer to quantitatively analyze gas products. As evident in Figure 1(d), CO gas was detected as a major product. On the basis of an E-pO plot, it has been reported that CO production from carbonate salt is thermodynamically feasible at the reaction temperature of 750°C in the potential range of -1.52 to +0.58 V vs. Ag/Ag_2SO_4 [7]. The concentration of the CO gas produced gradually increased with time, indicating that the cathode surface underwent dynamic changes during electrolysis.

To examine the effect of the current density on the product selectivity, FEs for carbon and CO production were calculated. As shown in Figure 1(e), the CO FE tended to increase as the current density decreased, while the FE for carbon production decreased. This implies that CO generation was favored over carbon production at low current densities and more positive potentials. This result agrees well with the thermodynamic expectation from the E-pO plot, where the onset potential of CO evolution is more positive than that of carbon production [7].

Chronopotentiometry experiments were conducted at 25 mA cm^{-2} for different borate concentrations to investigate the effect of borate concentration (Figure S1). The CO FE was determined to be 22.3%, 53.2%, and 88.0% for borate concentrations of 3, 5, and 7 mol%, respectively (Figure 1(f)). At higher borate concentrations, CO evolution was preferred, and carbon production was relatively suppressed. It has been reported that a borate additive not only participates in carbonate reduction to produce CO but also lowers the local concentration of O^{2-} anions owing to the existence of chemical equilibrium between BO_2^- and BO_3^{3-} as shown in Eq. (5). At low O^{2-} concentrations, E-pO plots have shown that CO generation is energetically preferred [7].

For the investigation of the effects of borate concentration and current density on the carbon morphology, SEM analysis of Ni cathodes was conducted after 2 h chronopotentiometry experiments. Figures 2(a)–2(d) show SEM images of carbon samples synthesized with borate concentrations of 0, 3, 5, and 7 mol% at a current density of 25 mA cm^{-2}. Irregularly shaped carbon particles with sizes in the range of 30-150 nm were mainly observed for borate concentrations of 0 and 7 mol%, whereas one-dimensional CNTs were found in the other samples. In particular, at the borate concentrations of 3 and 5 mol%, the CNT diameter was in the approximate ranges of 18-38 and 15-19 nm, respectively. These results show that the borate additive significantly changed the carbon morphology and that there is an optimal concentration range for CNT production. SEM analysis of carbon samples synthesized at different current densities of 10, 25, 50, and 100 mA cm^{-2} was also performed at a borate concentration of 3 mol% (Figures 2(e)–(g)). There was no carbon deposition at the current density of 10 mA cm^{-2}. However, interestingly, the CNTs were thicker at higher current densities. The diameter of CNTs increased

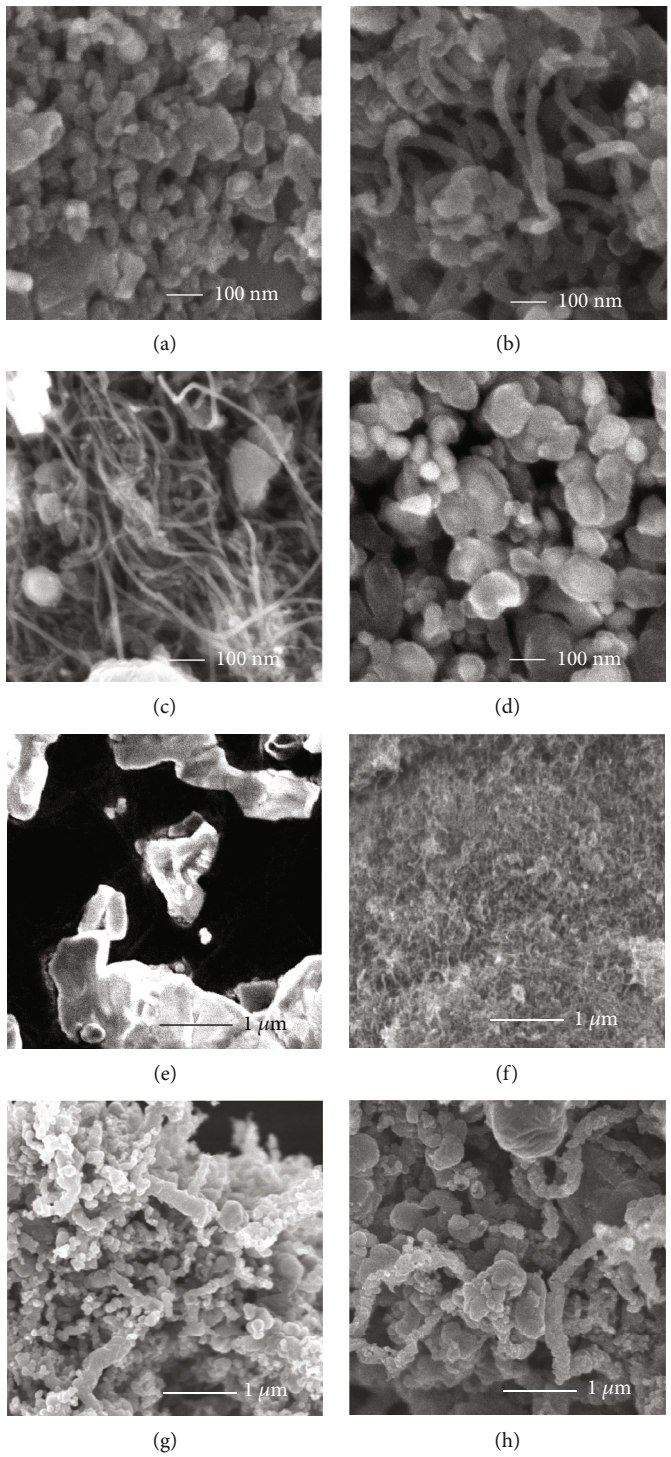

FIGURE 2: SEM images of nickel cathodes collected after 2 h of chronopotentiometry at 25 mA cm^{-2} in molten salt electrolytes with borate concentrations of (a) 0, (b) 3, (c) 5, and (d) 7 mol% under CO_2 flow of 50 mL min^{-1} at 750°C (scale bar: 100 nm). SEM images of nickel cathodes prepared at current densities of (e) 10, (f) 25, (g) 50, and (h) 100 mA cm^{-2} for a fixed borate concentration of 3 mol% (scale bar: 1 μm).

from 13-55 to 75-338 nm as the current density increased from 25 to 100 mA cm^{-2}. Thus, the dimensions of CNTs were closely related to the current density. According to previously reported research findings [40], an increase in current density is associated with an enlargement of the diameter of CNTs. This trend aligns with the results presented in Figure 2.

The nanostructural and compositional properties of a CNT sample prepared in this study were investigated using TEM analysis. Figures 3(a) and 3(b) show a TEM image of

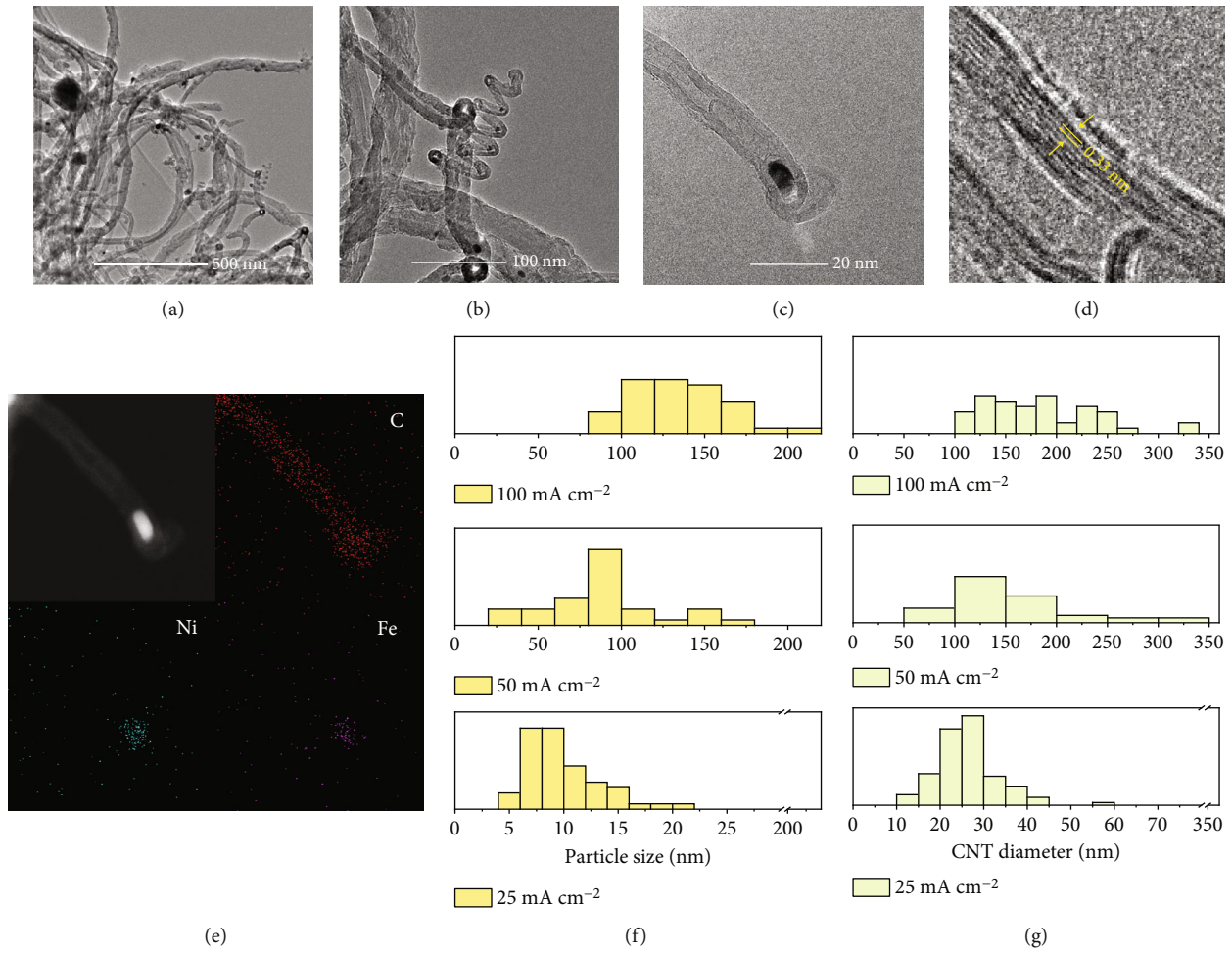

Figure 3: (a–c) High-resolution TEM and (d) lattice fringe images of a CNT sample collected after 2 h of chronopotentiometry at a current density of 25 mA cm^{-2} and a borate concentration of 3 mol%. (e) HAADF STEM-EDS mapping analysis results for the CNT sample. Size distributions of (f) seed particles and (g) CNTs measured after electrolysis for a borate concentration of 3 mol%.

the CNT sample prepared with 3 mol% borate and a current density of 25 mA cm^{-2}. The CNTs had a randomly entangled morphology, while the seed catalysts, observed as black particles, were sparsely distributed on the CNT surface. In a magnified view (Figure 3(b)), branched CNTs were found to have grown at the surface of some CNTs, forming a CNT network. Since metal seeds can serve as nucleation sites for CNT growth [2, 25, 34], it appears that extensive and continuous electrodeposition of the metal seed catalyst during constant-current electrolysis led to the formation of the CNT network.

The CNT nanostructure was further characterized through high-resolution TEM analysis of a representative CNT sample. As shown in Figure 3(c), the seed catalyst was precisely incorporated within the CNT, and the seed catalyst's diameter (5.2 nm) matched the CNT's internal diameter (5.2 nm). A lattice fringe image (Figure 3(d)) showed that the CNT wall was about 4 nm thick and contained less than 10 layers with an interlayer spacing of ~0.33 nm (d-spacing of the (002) crystallographic plane for graphitic carbon). Thus, the nanostructure resembled that of MWCNTs. These results showed that CNTs had been successfully synthesized.

High-angle annular dark-field scanning transmission electron microscopy–energy-dispersive X-ray spectroscopy (HAADF STEM-EDS) analysis was performed to determine the elemental distribution and composition of CNTs (Figure 3(e)). Carbon was found to be distributed over CNT surfaces, and the distributions of Ni and Fe elements matched well with that of the seed catalyst particles. For the CNT network, the atomic percentages of C, Ni, Fe, Cr, and O elements were ascertained to be 98.95, 0.27, 0.12, 0.10, and 0.56 at%, respectively (Figure S2 and Table S1). This indicates that Ni, Fe, and/or Ni-Fe alloy particles were the main seed catalysts involved with the nucleation and growth of CNTs. Since the Inconel 718 anode used in this work was a Ni-Fe-Cr alloy (55 : 17 : 21 wt%), it can be inferred that the metal particles incorporated into the CNTs originated from the anode. These results suggest that CNT growth occurred through a tip-growth mechanism [43, 44]. This mechanism involves the growth of CNTs below the metal catalyst onto a cathode substrate, with the CNTs pushing the metal catalyst in the opposite direction of the substrate as they continue to grow.

In molten salt-based CO_2 electrolysis, nucleation, and growth of CNTs can be promoted and controlled through seed supply by regulating anodic dissolution and the

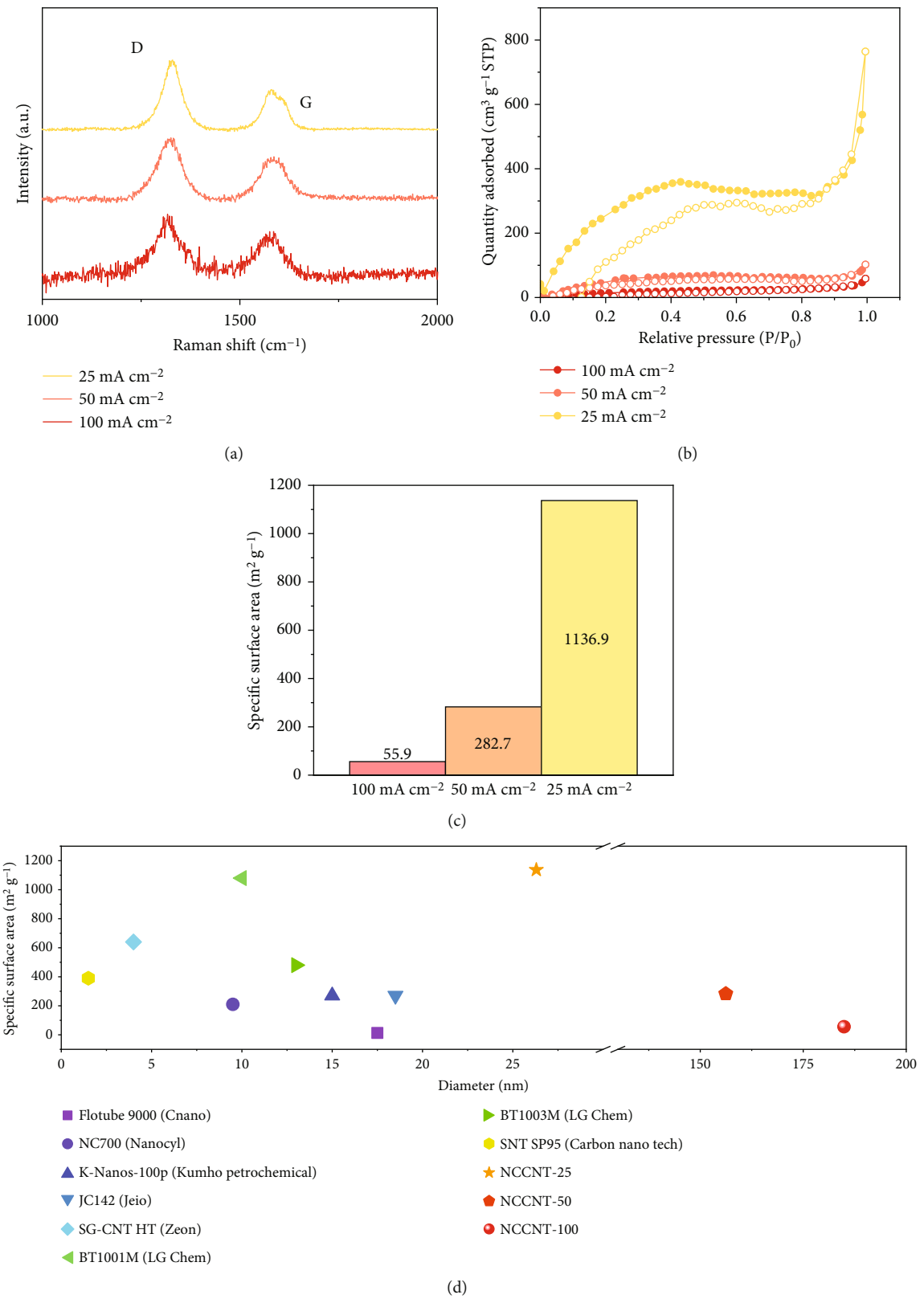

Figure 4: (a) The Raman spectra of CNTs prepared at current densities of 25, 50, and 100 mA cm^{-2} for a borate concentration of 3 mol%. (b) N_2 adsorption-desorption isotherms and (c) the corresponding specific surface area of the CNT products. (d) Plot of the specific surface area vs. the CNT diameter for different CNT products. Nucleation-controlled CNTs prepared with the three current densities are denoted by NCCNT-25, NCCNT-50, and NCCNT-100, and commercial CNT products obtained through chemical vapor deposition (CVD) methods are indicated by the model and company names.

cathodic deposition of the catalyst particles. A higher current density facilitates the formation of a larger seed catalyst at the cathode surface (Figure 3(f)), which is likely to lead to the growth of larger CNTs (Figure 3(g)). The size distribution of CNTs and seed particles was statistically analyzed by counting the number of CNTs formed, which was more than 100 (Figure S3). The CNT diameter was determined to be 26.3 ± 6.9, 156.2 ± 63.1, and 184.9 ± 55.8 nm at the current densities of 25, 50, and 100 mA cm^{-2}, respectively. The seed particle size at these current densities was 9.8 ± 3.3, 95.0 ± 39.2, and 135.2 ± 26.6 nm, respectively. The borate-containing electrolyte reveals a bright and distinct manifestation of metal particles in the carbon product, whereas seed particles were not easily found without the borate additive (Figure S4).

The Raman spectra were measured using a 633 nm laser to characterize the crystallinity of the CNT products prepared at different current densities (25, 50, and 100 mA cm^{-2}) with a borate concentration of 3 mol% (Figure 4(a)). The crystallinity of CNTs was determined as the intensity ratio between the *D* and *G* bands of graphitic carbon [45]. The *D* band indicates defective sp^3-hybridized carbon, while the *G* band represents plane sp^2-hybridized carbon [45, 46]. A higher *G*/*D* ratio implies higher crystallinity. The synthesized CNTs showed *G*/*D* ratios of 0.55, 0.69, and 0.74 at 25, 50, and 100 mA cm^{-2}, respectively. At higher current densities, the *G*/*D* ratio tended to slightly increase. Furthermore, the specific surface area of the synthesized CNTs was evaluated through BET analysis. The N_2 adsorption-desorption isotherms showed a type 4 pattern, indicating that the synthesized CNTs are mesoporous materials. And the specific surface area of CNTs increased with a decrease in the current density since the CNT diameter was directly proportional to the current density (Figure 4(b)). The BET surface area increased from 55.9 to 1136.9 $m^2 g^{-1}$ when the current density decreased from 100 and 25 mA cm^{-2} (Figure 4(c)). It was also identified that the XRD pattern of the CNT material shows a strong peak at ~26° corresponding to the (002) plane of graphitic carbon (Figure S5).

Various CNT materials prepared through molten salt-based CO_2 electrolysis have been previously reported. Their material properties, namely, the specific surface area, crystallinity (*G*/*D* ratio), and outer diameter, are presented in Table S2 [2, 25, 27, 35, 46, 47]. Compared with commercial CNT materials, the CNTs prepared in the current study had a considerably high surface area because of the nucleation-controlled synthesis process (Figure 4(d)). Furthermore, although commercial CNTs produced for industrial use by using the chemical vapor deposition (CVD) method have smaller diameters (<20 nm), our CNTs showed a higher specific surface area and comparable *G*/*D* ratios (Table S3). These results indicate that the electrochemically produced CNTs have promising properties and high potential for use in industrial fields.

4. Conclusions

In this study, the effect of borate concentration and current density on CNT synthesis through the electrochemical reduction of CO_2 in a molten salt electrolyte was investigated. The results show that the borate concentration plays a critical role in determining the carbon morphology and product selectivity. Specifically, when the borate concentration was as high as 7 mol%, CO generation predominated over carbon formation. Thus, at high borate concentrations, the formation of carbon materials, including CNTs, is significantly hindered. However, moderate borate concentrations (e.g., 3 and 5 mol%) are conducive to CNT growth. Without the borate additive (0 mol%), irregularly shaped carbon was mainly formed; however, carbon production was preferred over CO evolution. Since borate addition could facilitate the dissolution of the metal anode and the formation of a seed catalyst on the cathode, for small borate concentrations, nucleation and growth of CNTs could occur with the aid of the seed catalyst. Therefore, optimizing the borate concentration is important to synthesize CNTs while relatively suppressing CO evolution. Furthermore, the dimensions of the synthesized carbon materials were closely related to the current density. At a fixed borate concentration of 3 mol%, current densities of 25, 50, and 100 mA cm^{-2} resulted in the formation of CNTs with average diameters of approximately 26, 156.2, and 184.9 nm, respectively. Comprehensive TEM analyses showed that the seed catalyst particles, originating from anodic dissolution and deposition on the cathode surface, were smaller at lower current densities, resulting in the growth of CNTs with smaller diameters through a seed-mediated tip-growth mechanism. Future research should more clearly investigate the mechanisms behind seed-mediated CNT growth and conduct quantitative studies on how various factors influence the properties of CNTs. This study provides deep insights into the mechanism of CNT synthesis through molten-carbonate-salt-based electrochemical conversion.

Data Availability

The data used to support the findings of this study are included within the article and the supplementary information file.

Conflicts of Interest

The authors declare that they have no known competing financial interests or personal relationships that could have influenced the work reported in this paper.

Authors' Contributions

C.W.L. designed and directed the project. M.W.P. conducted the experiment. Both authors wrote the manuscript.

Acknowledgments

This work was supported by National Research Foundation of Korea (NRF) grants funded by the Korean government (MSIT) (RS-2023-00210114 and NRF-2022R1A4A1019296), by the KIST Institutional Program (Project No. 2V09760-23-021), and by the Circle Foundation (Project No. 2023 TCF Innovative Science Project-04).

Supplementary Materials

Figure S1: two-hour chronopotentiometry with different borate concentrations at a current density of 25 mA cm^{-2}. Figure S2: elemental intensity of CNTs, obtained from TEM-EDS analysis. Figure S3: SEM images used for obtaining the particle size and CNT diameter distribution plot. Images. Figure S4: SEM image of the carbon product for (a, b) Li_2CO_3-LiCl electrolyte and for (c, d) Li_2CO_3-LiCl-3 mol% $LiBO_2$ electrolyte. Figure S5: XRD analysis result of the CNT for Li_2CO_3-LiCl-3 mol% $LiBO_2$ electrolyte at current density of 25 mA cm^{-2}. Table S1: elemental ratio determined through SEM-EDS mapping. Table S2: specifications of CNT products obtained by earlier studies through molten salt electroreduction and CNTs prepared in the current study. Table S3: specifications of commercial CNTs and CNTs prepared in the current study. *(Supplementary Materials)*

References

[1] R. Jiang, M. Gao, X. Mao, and D. Wang, "Advancements and potentials of molten salt CO_2 capture and electrochemical transformation (MSCC-ET) process," *Current Opinion in Electrochemistry*, vol. 17, pp. 38–46, 2019.

[2] X. Liu, G. Licht, X. Wang, and S. Licht, "Controlled transition metal nucleated growth of carbon nanotubes by molten electrolysis of CO_2," *Catalysts*, vol. 12, no. 2, p. 137, 2022.

[3] S. K. Gupta and Y. Mao, "A review on molten salt synthesis of metal oxide nanomaterials: status, opportunity, and challenge," *Progress in Materials Science*, vol. 117, article 100734, 2021.

[4] Y. Sato, "Physical properties of high temperature molten salts," *ECS Transactions*, vol. 33, no. 7, pp. 145–157, 2010.

[5] Y. Chen, M. Wang, J. Zhang, J. Tu, J. Ge, and S. Jiao, "Green and sustainable molten salt electrochemistry for the conversion of secondary carbon pollutants to advanced carbon materials," *Journal of Materials Chemistry A*, vol. 9, no. 25, pp. 14119–14146, 2021.

[6] L. Hu, B. Deng, K. Du, R. Jiang, Y. Dou, and D. Wang, "Tunable selectivity and high efficiency of CO_2 electroreduction via borate-enhanced molten salt electrolysis," *IScience*, vol. 23, no. 10, article 101607, 2020.

[7] L. Hu, B. Deng, Z. Yang, and D. Wang, "Buffering electrolyte alkalinity for highly selective and energy-efficient transformation of CO_2 to CO," *Electrochemistry Communications*, vol. 121, article 106864, 2020.

[8] J. H. Park, J. Yang, D. Kim, H. Gim, W. Y. Choi, and J. W. Lee, "Review of recent technologies for transforming carbon dioxide to carbon materials," *Chemical Engineering Journal*, vol. 427, article 130980, 2022.

[9] J. Ren, A. Yu, P. Peng, M. Lefler, F. F. Li, and S. Licht, "Recent advances in solar thermal electrochemical process (STEP) for carbon neutral products and high value nanocarbons," *Accounts of Chemical Research*, vol. 52, no. 11, pp. 3177–3187, 2019.

[10] B. Deng, M. Gao, R. Yu, X. Mao, R. Jiang, and D. Wang, "Critical operating conditions for enhanced energy-efficient molten salt CO_2 capture and electrolytic utilization as durable looping applications," *Applied Energy*, vol. 255, article 113862, 2019.

[11] N. Dlamini, H. E. Mukaya, and D. Nkazi, "Carbon-based nanomaterials production from environmental pollutant byproducts: a review," *Journal of CO2 Utilization*, vol. 60, article 101953, 2022.

[12] D. Ji, Q. Jia, C. Zhu, W. Dong, H. Wu, and G. Wang, "A new, efficient conversion technology to transform ambient CO_2 to valuable, carbon-based fuel via molten salt electrochemistry," *Applied Sciences*, vol. 12, no. 17, p. 8874, 2022.

[13] F. Zhu, J. Ge, Y. Gao et al., "Molten salt electro-preparation of graphitic carbons," *Exploration*, vol. 3, no. 1, article 20210186, 2023.

[14] A. Yu, G. Ma, J. Ren, P. Peng, and F.-F. Li, "Sustainable carbons and fuels: recent advances of CO_2 conversion in molten salts," *ChemSusChem*, vol. 13, no. 23, pp. 6229–6245, 2020.

[15] M. Johnson, J. Ren, M. Lefler et al., "Carbon nanotube wools made directly from CO_2 by molten electrolysis: value driven pathways to carbon dioxide greenhouse gas mitigation," *Materials Today Energy*, vol. 5, pp. 230–236, 2017.

[16] S. Licht, X. Liu, G. Licht, X. Wang, A. Swesi, and Y. Chan, "Amplified CO_2 reduction of greenhouse gas emissions with C2CNT carbon nanotube composites," *Materials Today Sustainability*, vol. 6, article 100023, 2019.

[17] S. Shahidi and B. Moazzenchi, "Carbon nanotube and its applications in textile industry–a review," *Journal of the Textile Institute*, vol. 109, no. 12, pp. 1653–1666, 2018.

[18] A. Ali, S. S. Rahimian Koloor, A. H. Alshehri, and A. Arockiarajan, "Carbon nanotube characteristics and enhancement effects on the mechanical features of polymer-based materials and structures – a review," *Journal of Materials Research and Technology*, vol. 24, pp. 6495–6521, 2023.

[19] K. Kobashi, S. Ata, T. Yamada, D. N. Futaba, T. Okazaki, and K. Hata, "Classification of commercialized carbon nanotubes into three general categories as a guide for applications," *ACS Applied Nano Materials*, vol. 2, no. 7, pp. 4043–4047, 2019.

[20] R. Maheswaran and B. P. Shanmugavel, "A critical review of the role of carbon nanotubes in the progress of next-generation electronic applications," *Journal of Electronic Materials*, vol. 51, no. 6, pp. 2786–2800, 2022.

[21] Z. Xiong, Y. S. Yun, and H. J. Jin, "Applications of carbon nanotubes for lithium ion battery anodes," *Materials*, vol. 6, no. 3, pp. 1138–1158, 2013.

[22] B. J. Landi, M. J. Ganter, C. D. Cress, R. A. DiLeo, and R. P. Raffaelle, "Carbon nanotubes for lithium ion batteries," *Energy & Environmental Science*, vol. 2, no. 6, pp. 638–654, 2009.

[23] C. D. Casas and W. Li, "A review of application of carbon nanotubes for lithium ion battery anode material," *Journal of Power Sources*, vol. 208, pp. 74–85, 2012.

[24] X. M. Liu, Z. D. Huang, S. W. Oh et al., "Carbon nanotube (CNT)-based composites as electrode material for rechargeable Li-ion batteries: a review," *Composites Science and Technology*, vol. 72, no. 2, pp. 121–144, 2012.

[25] A. Douglas, R. Carter, M. Li, and C. L. Pint, "Toward small-diameter carbon nanotubes synthesized from captured carbon dioxide: critical role of catalyst coarsening," *ACS Applied Materials & Interfaces*, vol. 10, no. 22, pp. 19010–19018, 2018.

[26] X. Wang, X. Liu, G. Licht, B. Wang, and S. Licht, "Exploration of alkali cation variation on the synthesis of carbon nanotubes by electrolysis of CO_2 in molten carbonates," *Journal of CO2 Utilization*, vol. 34, pp. 303–312, 2019.

[27] X. Liu, G. Licht, and S. Licht, "The green synthesis of exceptional braided, helical carbon nanotubes and nanospiral platelets made directly from CO_2," *Materials Today Chemistry*, vol. 22, article 100529, 2021.

[28] D. Tang, H. Yin, X. Mao, W. Xiao, and D. H. Wang, "Effects of applied voltage and temperature on the electrochemical production of carbon powders from CO_2 in molten salt with an inert anode," *Electrochimica Acta*, vol. 114, pp. 567–573, 2013.

[29] H. Shi, M. Cai, W. Li et al., "Direct molten-salt electroreduction of CO_2 in porous electrodes," *Chemical Engineering Journal*, vol. 462, article 142240, 2023.

[30] X. Chen, H. Zhao, H. Xie et al., "Tuning the preferentially electrochemical growth of carbon at the "gaseous CO_2-liquid molten salt-solid electrode" three-phase interline," *Electrochimica Acta*, vol. 324, article 134852, 2019.

[31] E. Laasonen, M. Sorvali, V. Ruuskanen et al., "The effect of metal dissolution on carbon production by high-temperature molten salt electrolysis," *Journal of CO2 Utilization*, vol. 69, article 102390, 2023.

[32] J. Ren, M. Johnson, R. Singhal, and J. Licht, "Transformation of the greenhouse gas CO_2 by molten electrolysis into a wide controlled selection of carbon nanotubes," *Journal of CO2 Utilization*, vol. 18, pp. 335–344, 2017.

[33] J. Ren, F. F. Li, J. Lau, L. González-Urbina, and S. Licht, "One-pot synthesis of carbon nanofibers from CO_2," *Nano Letters*, vol. 15, no. 9, pp. 6142–6148, 2015.

[34] W. Han, Y. Bando, K. Kurashima, and T. Sato, "Boron-doped carbon nanotubes prepared through a substitution reaction," *Chemical Physics Letter*, vol. 299, no. 5, pp. 368–373, 1999.

[35] H. Wu, Z. Li, D. Ji et al., "One-pot synthesis of nanostructured carbon materials from carbon dioxide via electrolysis in molten carbonate salts," *Carbon N. Y.*, vol. 106, pp. 208–217, 2016.

[36] E. Laasonen, V. Ruuskanen, M. Niemelä, T. Koiranen, and J. Ahola, "Insights into carbon production by CO_2 reduction in molten salt electrolysis in coaxial-type reactor," *Journal of Environmental Chemical Engineering*, vol. 10, no. 1, article 106933, 2022.

[37] Z. Li, D. Yuan, H. Wu, W. Li, and D. Gu, "A novel route to synthesize carbon spheres and carbon nanotubes from carbon dioxide in a molten carbonate electrolyzer," *Inorganic Chemistry Frontiers*, vol. 5, no. 1, pp. 208–216, 2018.

[38] Q. Zhu, Y. Zeng, and Y. Zheng, "Overview of CO_2 capture and electrolysis technology in molten salts: operational parameters and their effects," *Industrial Chemistry & Materials*, vol. 1, no. 4, pp. 595–617, 2023.

[39] M. P. Nitzsche, L. Bromberg, and T. A. Hatton, "Capture and electrochemical reduction of CO_2 using molten alkali metal borates," *ACS Sustainable Chemistry & Engineering*, vol. 11, no. 30, pp. 11012–11018, 2023.

[40] A. Yu, G. Ma, L. Zhu et al., "Electrochemically controlled in situ conversion of CO_2 to defective carbon nanotubes for enhanced H_2O_2 production," *Nanoscale*, vol. 13, no. 37, pp. 15973–15980, 2021.

[41] Z. Kang, J. Xu, H. Liu, Y. Lin, X. Liu, and M. He, "Thermophysical properties of LiF–LiCl–Li_2CO_3 eutectic mixture/multi-walled carbon nanotubes for thermal energy storage," *Solar Energy Materials and Solar Cells*, vol. 241, p. 111744, 2022.

[42] M. Johnson, J. Ren, M. Lefler, G. Licht, J. Vicini, and S. Licht, "Data on SEM, TEM and Raman spectra of doped, and wool carbon nanotubes made directly from CO_2 by molten electrolysis," *Data in Brief*, vol. 14, pp. 592–606, 2017.

[43] D. Tang, K. Zheng, H. Yin, X. Mao, D. R. Sadoway, and D. Wang, "Electrochemical growth of a corrosion-resistant multi-layer scale to enable an oxygen-evolution inert anode in molten carbonate," *Electrochimica Acta*, vol. 279, pp. 250–257, 2018.

[44] A. Gohier, C. P. Ewels, T. M. Minea, and M. A. Djouadi, "Carbon nanotube growth mechanism switches from tip- to base-growth with decreasing catalyst particle size," *Carbon N. Y.*, vol. 46, no. 10, pp. 1331–1338, 2008.

[45] J. P. Tessonnier and D. S. Su, "Recent progress on the growth mechanism of carbon nanotubes: a review," *ChemSusChem*, vol. 4, no. 7, pp. 824–847, 2011.

[46] A. C. Ferrari and J. Robertson, "Interpretation of Raman spectra of disordered and amorphous carbon," *Physical Review B*, vol. 61, no. 20, pp. 14095–14107, 2000.

[47] P. Wang, Y. Liu, Z. Li et al., "Molten salts CO_2 transformation: lower energy input and high-yield carbon nanotubes production induced by zinc oxide," *Journal of the Electrochemical Society*, vol. 168, no. 8, article 083501, 2021.